Measurement of fluid-flow-velocity profile in turbid media by the use of optical Doppler tomography

Xiao-jun Wang, Thomas E. Milner, Zhongping Chen, and J. Stuart Nelson

Optical Doppler tomography is demonstrated to be a simple, accurate, and noncontact method for measuring the fluid velocity of laminar flow in small-diameter (~0.5-mm) ducts. Studies are described that utilize circular (square) plastic(glass) ducts infused with a moving suspension of polymer microspheres in air and buried in an optically turbid medium. The measurement of Doppler-shifted frequencies of backscattered light from moving microspheres is used to construct a high-resolution spatial profile of fluid-flow velocity in the ducts. © 1997 Optical Society of America

Key words: Optical Doppler tomography, Doppler shift, optically turbid media, fluid-flow profile, low-coherence interferometry.

1. Introduction

Measurements of fluid-flow velocity by the use of multigated ultrasound imaging[1] and laser Doppler velocimetry have found many applications in scientific research and industry. Although multigated ultrasound imaging can be used to resolve the velocity of flowing fluid at different positions within ducts, the mean Doppler frequency is easily altered by many factors and can be difficult to interpret.[2] Use of a highly coherent light source in laser Doppler velocimetry requires a specialized geometry (e.g., two intersecting beams) to achieve useful spatial resolution. More important, when the fluid or duct is highly scattering or buried in a turbid medium, the method is difficult to apply. Coherence techniques, based on the detection of the interference fringe intensity of light backscattered from a sample, have been successfully demonstrated for microstructural imaging in optically turbid media.[3–5]

Spatial resolution in interferometric flow-velocity sensors may be improved over conventional laser systems by the use of a low-coherence or broadband spectral source.[6] Meggit *et al*. have demonstrated a low-coherence fiber-optic Doppler anemometer by using both homodyne and heterodyne detection approaches.[7] Inasmuch as spatial resolution is directly dependent on the coherence length of the source light, reported longitudinal spatial resolution was approximately ~200 μm. We report the application of a conventional fiber-optic Michelson interferometer that uses a superluminescent diode (SLD) light source in combination with a focusing lens to give a significantly smaller coherent detection volume (i.e., $V_c = 5\ \mu m \times 5\ \mu m \times 15\ \mu m$) for fluid-flow-velocity measurements. Because the method employs optical low-coherence interferometry in combination with the Doppler effect,[8,9] we call this technique optical Doppler tomography (ODT). High-spatial-resolution measurements of fluid-flow-velocity profiles are reported in both circular and square and glass and plastic ducts infused with a moving suspension of polymer microspheres in doubly deionized water. The ducts are studied both in the air and buried in a turbid medium.

2. Methodology

Optical low-coherence interferometry is an established technique for assessing the position of static structures within turbid materials by the measurement of the interference fringe intensity of backscattered light.[8–10] Continuous near-infrared light ($\lambda_0 = 850$ nm) emitted by a SLD is coupled into a fiber-optic Michelson interferometer and split into two beams by a 2×2 fiber coupler (Fig. 1). SLD power in the input fiber of the interferometer is set at 1 mW. Optical power in the

The authors are with the Beckman Laser Institute and Medical Clinic, University of California–Irvine, Irvine, California 92715. X.-J. Wang is also with the Department of Physics, Georgia Southern University, Statesboro, Georgia 30460.

Received 15 August 1996; revised manuscript received 29 August 1996.

0003-6935/97/010144-06$10.00/0

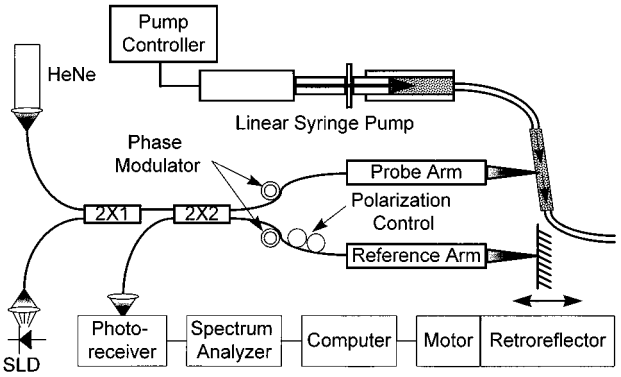

Fig. 1. Schematic of ODT instrumentation.

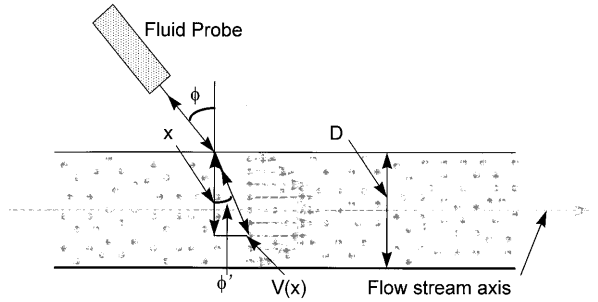

Fig. 2. Diagram of the probe light beam focused into duct and laminar fluid. ϕ and ϕ' represent angles between the flow velocity and the optical axis of incoming light in air and fluid, respectively; D is the inner dimension of the duct, x is the probe depth, and V is the fluid-flow velocity at position x.

reference arm of the interferometer is attenuated to 2 μW to reduce random light-intensity fluctuations[11] and thus achieve a higher signal-to-noise ratio.[12] Light from a He–Ne laser ($\lambda_0 = 632.8$ nm) is coupled into the interferometer by a 2×1 fiber coupler and serves as an aiming beam in the fluid probe. The optical phase of the SLD light in both the probe and the reference arms of the interferometer is modulated (1000 Hz) by a stretching fiber wrapped around piezoelectric cylinders expanded by a serrodyne (i.e., ramp) waveform. Stress–birefringence is used to match the polarization of the probe and the reference beams and thus optimize fringe contrast.

A test suspension consisting of polymer microspheres (diameter 2.062 ± 0.025 μm) in doubly deionized water (3.4×10^7 cm^{-3} concentration) or intralipid (0.25% concentration) is infused through the test duct at constant velocity by a linear syringe pump. A microlens terminating the fluid probe focuses light (NA = 0.22) within the duct to produce a 5-μm-diameter spot size. Light that is backscattered and Doppler shifted from moving microspheres in the fluid suspension recombines in the 2×2 fiber coupler with the light reflected from the reference mirror. The two beams interfere and give fringes only when their optical path-length difference is approximately less than or equal to the coherence length ($\lambda^2/\Delta\lambda \sim 16$ μm) of the SLD source light. Because the coherence envelope of the SLD source light yields a rapid phase decorrelation of the beams for path-length differences greater than the coherence length, high spatial resolution is achieved. Backscattered and Doppler-shifted light at a user-specified position can be detected by the scanning of either the reference mirror of the interferometer or by translation of the fluid probe. A photovoltaic detector (New Focus 2001) in combination with a spectrum analyzer (HP 8560E) is used to measure the power spectra of optical interference fringe intensity.

3. Results and Analysis

We set fluid velocity in our experiments by adjusting the speed of the linear syringe pump. The calculation of the Reynolds number[13] [N_R, Eq. (1)] allows differentiation between laminar and turbulent flow regimes:

$$N_R = \frac{VD\rho}{\eta} \tag{1}$$

where V is the fluid-flow velocity, D is the duct's inner dimension, ρ is the solvent density, and η is the dynamic viscosity of the solvent. In our experiments, $V < 0.3$ cm/s, $D < 0.1$ cm, $\rho = 1$ g/cm^3, and η (H_2O) = 0.010 (g/cm s), giving $N_R < 3$. Because the Reynolds number is much less than the threshold value for turbulence ($N_R \leq 3000$), the flow is laminar. We assume a coordinate system with a z axis parallel to the long axis of the duct so that fluid velocity at all points within the flow is dependent on the lateral position [i.e., $V(x, y)$]. Furthermore, we assume that the fluid infusion pressure is constant over a cross-sectional area perpendicular to the z axis and that a constant gradient exists along the axis of the duct so that the Navier–Stokes equation for laminar flow applies:

$$\frac{\partial^2 V}{\partial x^2} + \frac{\partial^2 V}{\partial y^2} = -\frac{\Delta p}{\eta \Delta L}, \tag{2}$$

where Δp is the pressure difference along a length (ΔL) of the duct.

Because laminar flow is one dimensional, a solitary fluid probe is sufficient to investigate flow velocity at a user-specified position within the duct. To detect Doppler-shifted signals, orientation of the fluid probe relative to the duct is fixed to give a nonzero component of flow velocity parallel to the incoming light propagation vector. In this arrangement (Fig. 2), a simple geometric relationship exists between scanning depth in the duct (x), reference mirror position (R), and orientation of the fiber probe (ϕ'):

$$x = \frac{R \cos(\phi')}{n}, \tag{3}$$

where ϕ' represents the angle between the flow velocity and the optical axis of incoming light in fluid, n is the refractive index of the solvent, and we assume that $R = 0$ corresponds to a zero path-length difference when the beam waist in the fluid probe is positioned at the inner wall of the duct. When $V(x, y)$ is measured, the position of the beam waist is fixed on the inner duct

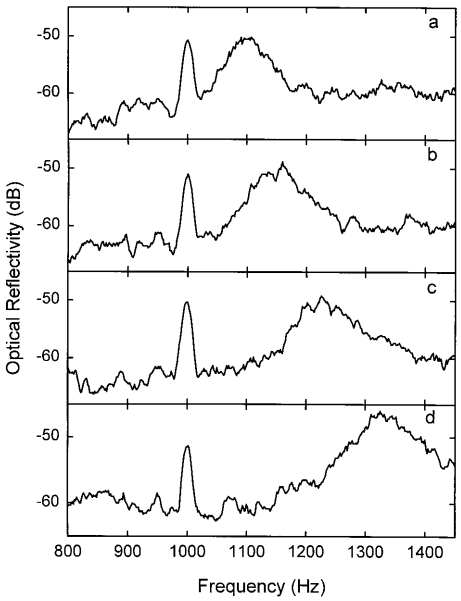

Fig. 3. Power spectra of four flow velocities [a, 188; b, 287; c, 423; d, 620 (μm/s)] at a single position in a square glass duct (curves offset by 20 dB). The bandwidth resolution of the spectrum analyzer is 10 Hz.

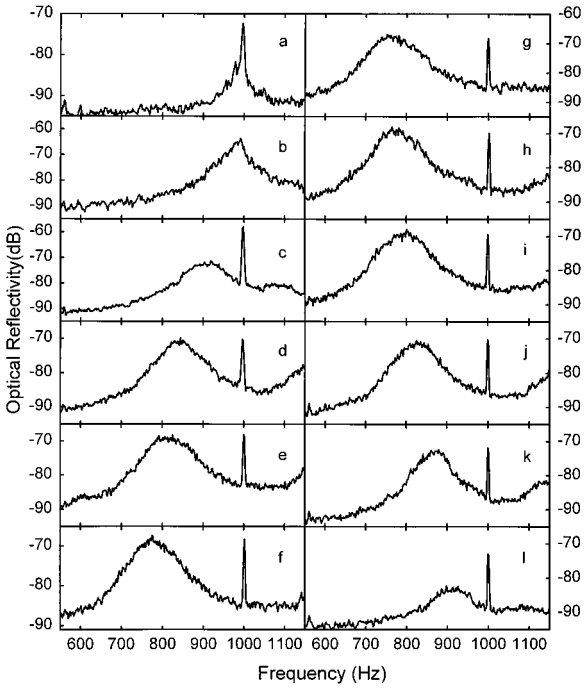

Fig. 4. Power spectra of 12 flow velocities [a, 14; b, 26; c, 134; d, 228; e, 268; f, 323; g, 341; h, 328; i, 300; j, 254; k, 191; l, 122 (μm/s)] at sequential positions along a linear grid [a, 5; b, 6; c, 37; d, 73; e, 110; f, 147; g, 183; h, 220; i, 257; j, 294; k, 330; l, 367 (μm)] coincident with the diameter of a circular glass duct. The bandwidth resolution of the spectrum analyzer is 3 Hz.

wall and data are recorded while the reference mirror of the interferometer is scanned. The reference mirror is positioned so that the zero path-length location of the two beams occurs at a scanning depth (x) specified in Eq. (3) and is centered on the spatial coherence envelope of the SLD source light where interference fringe intensity is maximum. Translating the reference mirror of the interferometer to a user-specified second position allows the detection of interference fringe intensity of backscattered light at a corresponding position (x) specified in Eq. (3).

Four power spectra of interference fringe intensities (Fig. 3) are recorded at a single position in a square glass duct for increasing flow velocity. Doppler-shifted and base modulation (1000-Hz) frequencies are represented, respectively, by wide and narrow peaks. Determination of the fluid-flow-velocity profile $V(x)$ of the fluid is derived from local measurement of the Doppler shift $\Delta f(x)$ over a linear grid perpendicular to the flow:

$$V(x) = \frac{\Delta f(x)\lambda_0}{2\cos(\phi)}. \tag{4}$$

Figure 4 shows Doppler-shifted power spectra at sequential positions along a linear grid coincident with the diameter of a glass circular duct. The fluid-flow velocity at the pump is fixed, and measurements correspond to successively deeper positions (i.e., greater velocities) toward the center of the duct.

A. Flow in Circular Glass Ducts

To analyze the flow, we assume a circular coordinate system with the origin at the center of the duct so that the Navier–Stokes equation [Eq. (2)] becomes

$$\frac{1}{r}\frac{\mathrm{d}}{\mathrm{d}r}\left(r\frac{\mathrm{d}V}{\mathrm{d}r}\right) = -\frac{\Delta p}{\eta \Delta L}. \tag{5}$$

Assuming a nonslip boundary condition [$V(r = d/2) = 0$] at each point on the inner duct wall, Eq. (5) can be solved exactly. The solution for the fluid-flow velocity $V(r)$ at radial position r has a parabolic form:

$$V(r) = \frac{d^2\Delta p}{16\eta\Delta L}\left[1 - \left(\frac{2r}{d}\right)^2\right]. \tag{6}$$

Experiments were completed that measure the fluid-flow-velocity profile in circular glass ducts with an inner diameter of $d = 400$ μm. Fluid-flow velocity was measured at any position x within the duct by the appropriate positioning of the reference mirror of the interferometer. Doppler shifts were measured at a point on the central axis of a circular duct where maximum fluid-flow velocity was found and plotted (Fig. 5) versus corresponding flow speeds $V_{\max}$ deduced from Eq. (7):

$$V_{\max} = C_R\frac{A_{\mathrm{pump}}}{A_{\mathrm{duct}}}V_{\mathrm{pump}}, \tag{7}$$

where A_{pump} and A_{duct} are the cross-sectional areas of the syringe pump and the probed duct, respectively, V_{pump} is the syringe pump speed, and constant C_R is the ratio of maximum to average speeds across the

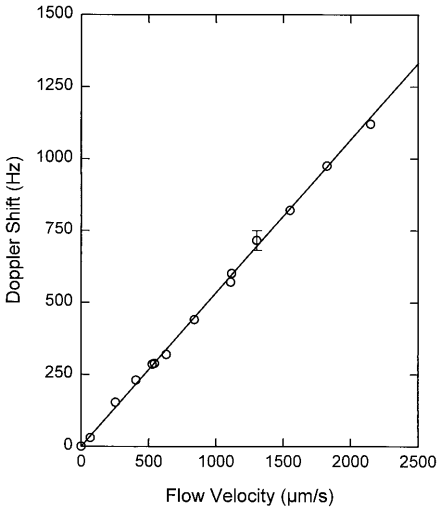

Fig. 5. Linear relationship between maximum fluid flow velocity V and measured Doppler shift Δf in a circular glass duct.

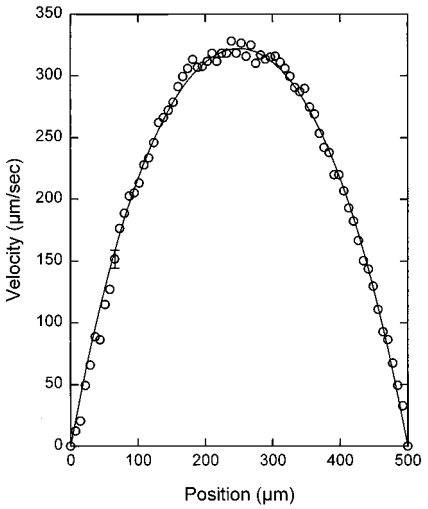

Fig. 7. Experimental (circles) and theoretical (solid curve) fluid-flow-velocity profiles in a square glass duct.

cross section of the duct. The value of C_R depends on the cross-sectional geometry of the duct; for a circular cross section, $C_R = 2$. The solid curve in Fig. 5 represents a least-squares linear fit to measured values. The incidence angle (Fig. 2) calculated from the slope in Fig. 4 is consistent with the value measured directly ($\phi = 73°$).

To deduce the fluid-flow-velocity profile, the Doppler shift was measured over a grid of points lying on a diameter of the circular duct [Fig. 6 (circles)]. The solid curve represents a least-squares fit based on Eq. (6). Fluid-flow-velocity uncertainty $\Delta V/V \sim 7\%$ was due to measurement errors in the Doppler shift Δf and incidence angle ϕ and was consistent with that computed from the mean variance between measured and fitted velocities.

B. Flow in Square Glass Ducts

We examined flow in a square duct (inner dimension D) and used a coordinate system with the origin coincident with one corner of the cross section. As in the analysis of the circular duct, we required a nonslip boundary condition at the inner wall so that

$$V(x = 0, y) = V(x = D, y) = V(x, y = 0) = V(x, y = D) = 0. \quad (8)$$

The fluid-flow-velocity profile along a central axis $[V(x, y = D/2)]$ is found by the solution of the Navier–Stokes equation with a Fourier series expansion[14]:

$$V\left(x, y = \frac{D}{2}\right) = \frac{16D^2\Delta p}{\pi^4 \eta \Delta L} \sum_{n=2i+1}^{\infty} \sum_{m=2j+1}^{\infty} \times \frac{\sin(n\pi/2)\sin(m\pi x/D)}{nm(n^2 + m^2)}, \quad i, j = 0, 1, 2 \ldots . \quad (9)$$

The fluid-flow-velocity profile (circles in Fig. 7) was measured along a linear grid over a central axis $[V(x, y = D/2)]$ perpendicular to the walls of a glass duct with a square cross section; the probed position in the duct was computed from Eq. (2). A fit to the collected data was computed (solid curve) from Eq. (9) with $\Delta p/\Delta L$ as a free parameter. The average fluid-flow velocity over the central axis (217 μm/s) as computed from measured data is in good agreement with that computed (212 μm/s) from Eqs. (7) and (9) (3.7×10^{-2} cm^3/s) and was within the uncertainty because of measurement errors of ϕ and Δf.

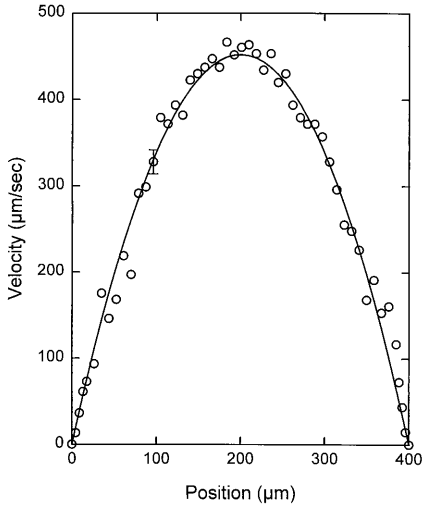

Fig. 6. Experimental (circles) and theoretical (solid curve) fluid-flow-velocity profiles in a circular glass duct.

C. Fluid Flow in a Scattering Duct Buried in Optically Turbid Media

An important advantage of low-coherence techniques over conventional Doppler flowmetry is the ability to detect and measure the flow velocity of moving constituents in optically turbid media. Laser Doppler or dual-beam cross-correlation techniques depend on a well-defined cross-beam profile and are applied only to transparent media and fluid to determine flow-

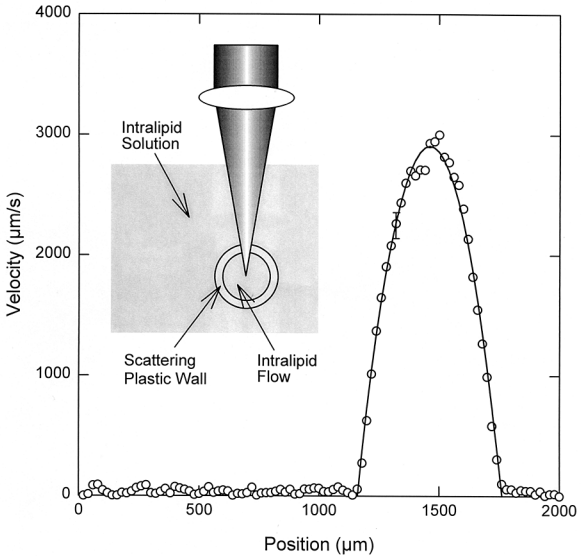

Fig. 8. Experimental (circles) and theoretical (solid curve) fluid-flow-velocity profiles along the vertical diameter in a diffusive plastic duct (circular) buried in a highly scattering intralipid solution. The inset is a schematic setup of the sample and the probe beam.

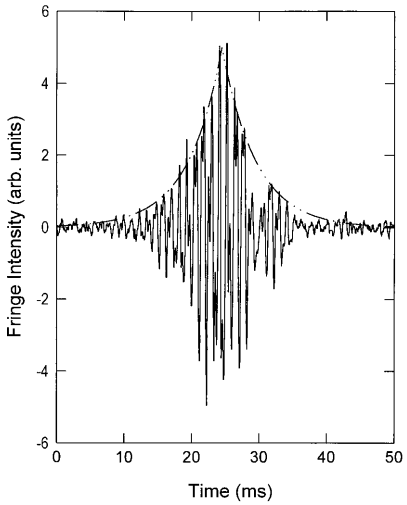

Fig. 9. Solid curve shows the measured interference fringe intensity of single microsphere passing through the coherent detection volume. The dashed–dotted curve shows the best fit to a double-sided exponential function.

velocity distribution. ODT is based on the detection of interference fringe intensity of light that is backscattered from a sample and has the ability to probe the underlying flow at a user-specified depth in a turbid medium. Figure 8 shows the intralipid flow-velocity profile (circles) along the vertical diameter within a scattering plastic circular duct, which is buried in the same intralipid solution (0.25% concentration, $\mu_s \sim 4.5\ \mathrm{cm}^{-1}$) at a depth of more than 1 mm (inset, Fig. 8). The background represents the non-Doppler-shifted light scattered from static intralipids outside the duct and the plastic wall. The solid curve represents a theoretical fit based on Eq. (6) and is consistent with experimental data. Fluid-flow-velocity measurement uncertainty $\Delta V/V$ is 8%.

4. Discussion and Conclusions

Magnitude and broadening of the Doppler shift in ODT experiments are dependent on a number of factors: (1) concentration and flow velocity of the microspheres, (2) position and size of the coherent detection volume, and (3) NA and orientation of the probe beam.

The frequency at which individual particles pass through the coherent detection volume is determined by microsphere concentration c and fluid-flow velocity V. Interference fringe intensity that represents the passage of a single microsphere through the coherent detection volume (Fig. 9) is amplitude modulated by a window function $w(t)$. The time-dependent variation of the function is related to backscattered light amplitude from a single microsphere at various positions within the light beam. Our experiments with dilute suspensions of polystyrene microspheres indicate that $w(t)$ is accurately approximated by a double-sided exponential function:

$$w(t) = \begin{cases} w_0 \exp(t - t_0)/\Delta t & t < t_0 \\ w_0 \exp -(t - t_0)/\Delta t & t > t_0 \end{cases}. \qquad (10)$$

The use of a best fit to $w(t)$ for data in Fig. 9 gives $\Delta t =$ 5 ms. In the frequency domain, amplitude modulation by $w(t)$ is equivalent to convolution by the Fourier transform of the window function $W(f)$ and results in the broadening of the Doppler-shifted peak. The Fourier transform of a double-sided exponential is a Lorentzian function. The spectral width δf of the function is inversely proportional to the time duration (Δt) required for passage of a single particle through the coherent detection volume (i.e., $\delta f \sim 100$ Hz). Because microspheres remain in the volume for a shorter duration at greater flow rates, an increase in the spectral width δf of the Doppler peak is observed at higher velocities for equivalent coherent detection volumes.

The position and the size of the coherent detection volume also affect ODT measurements. In our experiments, the beam-waist position is fixed on the inner duct wall so that the size of the coherent detection volume can vary when fluid-flow velocity is being measured at deeper positions in the duct. Spectral widths of Doppler-shifted peaks symmetrically positioned about the z axis in the circular conduit (Fig. 4) indicate that the size of the coherent detection volume does not vary considerably with depth x. By adjusting the position of reference mirror, we can track the focus of the probe beam and localize the coherent detection volume near the focal point. This adjustment may increase the sensitivity and decrease the lateral extent of the coherent detection volume when deeper positions are probed.

When scanning through a turbid medium, although the intensity of backscattered light drops exponentially (Fig. 10), the velocity profile, as shown in Fig. 8, is clearly

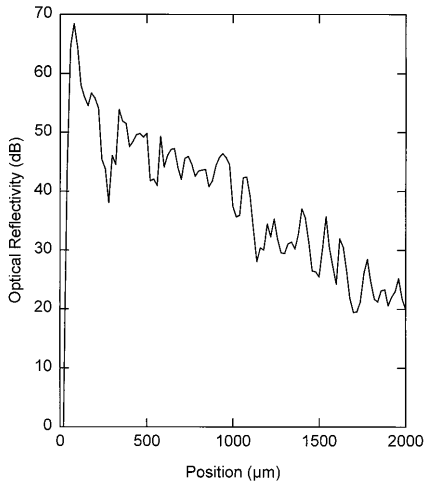

Fig. 10. Exponential decay of interference fringe intensity versus depth in a turbid intralipid solution.

resolved because the collected signal is almost entirely due to Doppler-shifted backscattered light from flowing intralipid within the coherence detection volume. As a result, a substantially higher spatial resolution of velocity flow is obtained compared with that of conventional laser Doppler flowmetry.

Finally, light scattered from an individual microsphere is dependent on both the beam profile and the relative position of the particle. Gouesbet and co-workers have developed a generalized Lorentz–Mie theory to describe scattering by a spherical particle at any position in an arbitrary incident light beam.[15,16] Because backscattered light amplitude from a single microsphere is dependent on the angular variation of scattered radiation and subsequent collection by a finite-sized aperture, incorporation of the generalized Lorentz–Mie formalism into the analysis should give a more realistic and accurate understanding of ODT theory.

When the optical properties of the test fluid or duct can be controlled, a mathematical relationship may exist between diameter, refractive index, and concentration of the microspheres for optimum fluid-flow-velocity measurements. If the microsphere diameter is small compared with the optical wavelength, backscattered light intensity generally increases; therefore reducing the size of the particles may improve the signal-to-noise ratio in some geometries. The refractive indices of the solvent n and of the spheres n' also affect measurements. When n'/n is near unity, the signal is reduced. When the ratio is higher, however, backscattered light intensity can increase significantly. A more complete theory that incorporates the effects of multiple scattering is necessary to analyze flow velocity in optically turbid media or at greater particle concentrations. ODT has many potential applications in science and industry and provides a simple, effective, and easily adapted technique for the assessment of fluid-flow velocity within ducts buried in optically turbid media.

The authors thank Wayne Sorin and Gerald Lucassen for helpful discussions and Wen Wang, Rupali P. Dhond, and Michael Chang for technical assistance. This project is supported through an academic equipment grant from Hewlett-Packard Laboratories and a postdoctoral fellowship (for X.-J. Wang) and independent research grants (for J. S. Nelson and T. E. Milner) from the Whitaker Foundation (9996) and the U.S. National Institutes of Health. Institute support from the U.S. Department of Energy, the U.S. Office of Naval Research, the U.S. National Institutes of Health, and Beckman Laser Institute Endowment is also gratefully acknowledged.

References

1. J. V. Chapman and G. R. Sutherland, "Blood flow measurements by Doppler ultrasound," in *The Noninvasive Evaluation of Hemodynamics in Congenital Heart Disease* (Kluwer, Dordrecht, The Netherlands, 1990), Chap. 3, pp. 55–66.
2. P. A. J. Bascom and R. S. C. Cobbold, "Effects of transducer beam geometry and flow velocity profile on the Doppler power spectrum—a theoretical study," Ultrasound Med. Biol. **16,** 279–295 (1990).
3. X. J. Wang, T. E. Milner, M. C. Chang, and J. S. Nelson, "Group refractive index measurement of dry and hydrated type I collagen films using optical low-coherence reflectometry," J. Biomed. Opt. **1,** 212–216 (1996).
4. G. J. Tearney, M. E. Brezinski, J. F. Southern, B. E. Bouma, M. R. Hee, and J. G. Fujimoto, "Determination of the refractive index of highly scattering human tissue by optical coherence tomography," Opt. Lett. **20,** 2258–2260 (1995).
5. J. A. Izatt, M. R. Hee, G. M. Owen, E. A. Swanson, and J. G. Fujimoto, "Optical coherence microscopy in scattering media," Opt. Lett. **19,** 590–592 (1994).
6. Y. N. Ning, K. T. V. Grattan, and A. W. Palmer, "Fiber-optic interferometric systems using low-coherence light sources," Sensors Actuators **30,** 181–192 (1992).
7. B. T. Meggit, W. J. O. Boyle, K. T. V. Grattan, A. W. Palmer, and Y. N. Ning, "Fiber optic anemometry using an optical delay cavity technique," in *Fiber Optics '90*, P. McGeehin, ed., Proc. SPIE **1314,** 321–326 (1990).
8. J. M. Schmitt, A. Knuttel, and R. F. Bonner, "Measurement of optical properties of biological tissues by low-coherence reflectometry," Appl. Opt. **32,** 6032–6042 (1993).
9. X. J. Wang, T. E. Milner, and J. S. Nelson, "Characterization of fluid flow velocity by optical Doppler tomography," Opt. Lett. **20,** 1337–1339 (1995).
10. X. J. Wang, T. E. Milner, S. A. Newton, R. P. Dhond, W. V. Sorin, and J. S. Nelson, "Characterization of human scalp hairs by optical low-coherence reflectometry," Opt. Lett. **20,** 524–526 (1995).
11. J. Goodman, *Statistical Optics* (Wiley, New York, 1985), p. 157.
12. W. V. Sorin and D. M. Baney, "A simple intensity noise reduction technique for optical low-coherence reflectometry," IEEE Photon. Technol. Lett. **4,** 1404–1406 (1992).
13. L. D. Landau and E. M. Lifshitz, *Fluid Mechanics*, 2nd ed. (Pergamon, Oxford, 1987), Chap. 2.
14. M. Spiga and G. L. Morini, "A symmetric solution for velocity profile in laminar flow through rectangular ducts," Int. Comm. Heat Mass Transfer **21,** 469–475 (1994).
15. G. Gouesbet, B. Maheu, and G. Gréhan, "Light scattering from a sphere arbitrarily located in a Gaussian beam, using a Bromwich formulation," J. Opt. Soc. Am. A **5,** 1427–1443 (1988).
16. B. Maheu, G. Gouesbet, and G. Gréhan, "A concise presentation of the generalized Lorentz–Mie theory for arbitrary location of the scatterer in an arbitrary incident profile," J. Opt. **19,** 59–67 (1988).